Supercurrent in the Presence of Direct Transmission and a Resonant Localized State

Vukan Levajac,[1] Hristo Barakov,[2] Grzegorz P. Mazur,[1] Nick van Loo,[1] Leo P. Kouwenhoven,[1] Yuli V. Nazarov,[2,*] and Ji-Yin Wang[1,3,†]

[1]QuTech and Kavli Institute of Nanoscience, Delft University of Technology, 2600 GA Delft, The Netherlands
[2]Kavli Institute of Nanoscience, Delft University of Technology, 2628 CJ Delft, The Netherlands
[3]Beijing Academy of Quantum Information Sciences, 100193 Beijing, China

(Received 8 October 2023; revised 25 January 2024; accepted 2 April 2024; published 25 April 2024)

We study the current-phase relation (CPR) of an InSb-Al nanowire Josephson junction in parallel magnetic fields up to 700 mT. At high magnetic fields and in narrow voltage intervals of a gate under the junction, the CPR exhibits π shifts. The supercurrent declines within these gate intervals and shows asymmetric gate voltage dependence above and below them. We detect these features sometimes also at zero magnetic field. The observed CPR properties are reproduced by a theoretical model of supercurrent transport via interference between direct transmission and a resonant localized state.

DOI: 10.1103/PhysRevLett.132.176304

A Josephson junction (JJ) consists of two superconductors (S) and a weak link that supports transport of Cooper pairs in the form of a nondissipative supercurrent [1]. If the weak link is a normal conductor (N), Andreev levels are formed inside the junction and mediate the supercurrent [2]. Semiconductor SNS-JJs are widely used to study the influence of their tunable properties on the Andreev spectrum and supercurrent. This is evident in multiple superconducting phenomena, including topological superconductivity [3–10], the anomalous Josephson effect [11–15], and the Josephson diode effect [16–23]. SNS-JJs also have attractive applications in gate-tunable superconducting qubits [24–26] and Andreev spin qubits [27–32].

A π-shift in the current-phase relation (CPR) of a JJ can occur due to spin splitting of the Andreev levels in an external magnetic field [11,12]. In the presence of Coulomb interaction, the supercurrent direction can depend on the junction parity, and $0-\pi$ transitions may occur even at zero field [33–36]. These phenomena have been studied for quantum-dot-based SNS-JJs in semiconducting nanowires [37–41], carbon nanotubes [42–44], and two-dimensional electron gases [45]. In hybrid nanowire JJs, the CPR has been measured only at low magnetic fields (tens of mT). Studying CPR in high magnetic fields is motivated by various proposals for detecting a topological phase transition by supercurrent measurements in hybrid nanowire JJs [5,7,46,47].

In this Letter, we study the CPR of a hybrid InSb-Al nanowire JJ embedded into a superconducting quantum interference device (SQUID) at unprecedentedly high parallel magnetic fields, exceeding 700 mT. At zero field, localized states in the junction are observed as resonances in the normal-state conductance. When these states become involved in the superconducting transport as they are tuned close to the Fermi energy by a gate under the junction, the supercurrent exhibits asymmetric amplitude modulation by the gate. In these gate intervals at zero field, either pairs of $0-\pi$ transitions give rise to π regions in the CPR, or the supercurrent is enhanced with constant phase. We further investigate the CPR by increasing parallel magnetic field and find that high fields can enlarge the π regions or drive new $0-\pi$ transitions. In order to understand these phenomena, we develop a model involving a transmission channel and a localized resonant state inside a single nanowire JJ. This model can reproduce the main interesting features observed in the experiment by considering the interference between the transmission channel and the localized state. This interference effect of supercurrent represents a novel, superconducting version of the well-known Fano effect [48].

The nanowire SQUID is introduced in Fig. 1(a) (left). Two InSb-Al nanowire Josephson junctions, JJ1 and JJ2, are enclosed in a superconducting Al loop. The Al layout is obtained through the shadow-wall lithography [49–51]. An enlargement of JJ1 is displayed in Fig. 1(a) (right). The junction is ~40 nm long and its electrochemical potential is controlled by an underlying gate with a voltage V_{G1}. The other two underlying gates with voltages V_{L1} and V_{R1} predominantly tune the nanowire sections covered by the left and right lead. JJ2 has nominally the same design as JJ1. An in-plane magnetic field B_z is applied parallel to JJ1 and the flux through the loop is introduced by an out-of-plane magnetic field B_y. For more details of the device fabrication, see our recent work [51].

We characterize the SQUID by applying a bias current I_b and measuring a voltage drop V across the SQUID while sweeping the flux through the loop. The measurements are performed at $B_z = 0$ mT and $B_z = 600$ mT [Fig. 1(b)]. Aside from the measurements in the 2D maps, a setup for switching current measurements in a fast way is employed

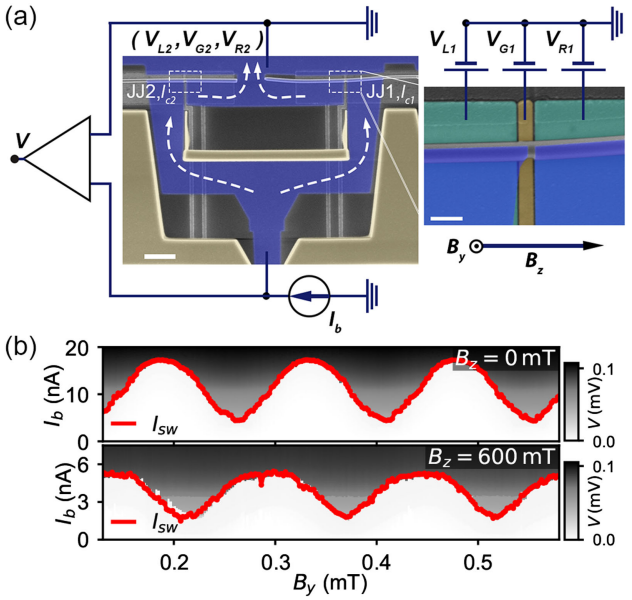

FIG. 1. (a) False-colored SEM image of the nanowire SQUID (left, scale bar 1 μm) and an enlargement of one arm (right, scale bar 100 nm). Dielectric shadow walls (yellow) define the two Josephson junctions (JJ1 and JJ2, critical currents I_{c1} and I_{c2}) in two InSb nanowires, and the superconducting Al (blue) loop on the substrate. White arrows indicate the current directions along the two SQUID arms between the source and drain connected in the four-terminal setup. JJi is coupled to three underlying gates at voltages V_{Li}, V_{Gi}, and V_{Ri} (i = 1,2). Magnetic fields B_z and B_y are applied along JJ1 and out of plane, respectively. (b) V as a function of I_b and B_y at $B_z = 0$ mT and $B_z = 600$ mT, overlapped by I_{sw} traces (red). The gate settings are $V_{G1} = 2.36$ V, $V_{L1} = V_{R1} = 1.5$ V, $V_{G2} = 2.88$ V. and $V_{L2} = V_{R2} = 1.75$ V.

[22,52]. For each B_y, a switching current value is recorded as the I_b value for which the SQUID switches from the superconducting to the resistive regime [53]. Such obtained $I_{sw}(B_y)$ dependences (red traces) overlap well with the 2D maps in Fig. 1(b), demonstrating the accuracy of the fast measurement setup; hence, we employ them in the rest of this work. The SQUID oscillations at high B_z confirm the resilience of supercurrent interference against large magnetic fields [51]. At zero magnetic field, we use the gates to tune the critical currents of JJ1 and JJ2 so that $I_{c2} \gg I_{c1}$. JJ2 then serves as the reference junction and the CPR of JJ1 is directly obtained from an $I_{sw}(B_y)$ trace. In our SQUID, B_z simultaneously suppresses $I_{c1,2}$, and a highly asymmetric SQUID configuration is not always reachable at high B_z. In spite of this, a $0-\pi$ transition in JJ1 still causes a half-period shift in the $I_{sw}(B_y)$ trace.

We first pinch off the reference arm and measure the differential conductance dI/dV_b of JJ1 in a two-terminal setup with the standard lock-in configuration [53]. In Fig. 2(a), dI/dV_b at $B_z = 0$ mT is shown as a function of a bias voltage V_b and V_{G1}. By finding the positions of the coherence peaks in the horizontal line cut, the superconducting gap of the leads $\Delta \sim 0.23$ meV is extracted. In the normal-state transport ($|V_b| > 2\Delta/e$), resonances in dI/dV_b (red dashed line) indicate the presence of a state localized in the junction. We estimate its charging energy as $U < 4$ meV $\sim 16\Delta$ and its coupling to the leads as $\Gamma \sim 1$ meV $\sim 4\Delta$ [53]. The features of superconducting transport ($|V_b| < 2\Delta/e$) exhibit strong modulation as the localized state approaches the in-gap energies and contributes to the superconducting transport. In order to investigate the influence of the localized state on the supercurrent, we turn on the reference arm and use the SQUID configuration to investigate the CPR.

Figure 2(b) displays I_{sw} of the SQUID as a function of B_y and V_{G1}. Three distinct regions can be identified, with the middle region being π-shifted (π region) relative to the regions below and above (0 regions). Noticeably, the π region occurs in the same V_{G1} interval in which the localized state is tuned below the superconducting gap

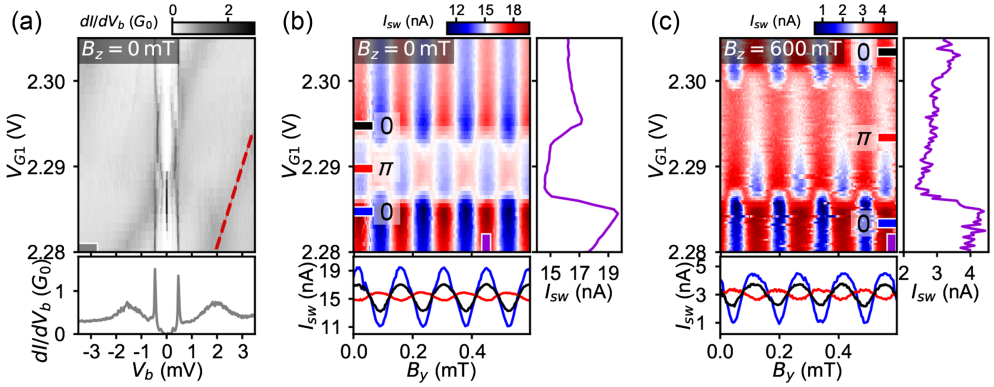

FIG. 2. (a) dI/dV_b as a function of V_b and V_{G1} at $B_z = 0$ mT and $V_{L1} = V_{R1} = 1.5$ V. JJ2 is pinched off by setting $V_{G2} = V_{L2} = V_{R2} = 0$ V. A line cut (gray) with sharp coherence peaks and broad resonance (red dashed line) peaks is shown below. (b) I_{sw} as a function of B_y and V_{G1} at $B_z = 0$ mT and $V_{L1} = V_{R1} = 1.5$ V. JJ2 is turned on by setting $V_{G2} = 2.88$ V and $V_{L2} = V_{R2} = 1.75$ V. Horizontal line cuts (red, blue, and black) are shown below and a vertical line cut (purple) is displayed on the right. (c) Same as (b) but for $B_z = 600$ mT.

in Fig. 2(a). Three horizontal line cuts demonstrate that the supercurrent declines inside the π region as its line cut has the smallest amplitude. Furthermore, there is an asymmetric gate voltage dependence of the supercurrent amplitude below and above the π region, as confirmed by the vertical line cut. Upon applying $B_z = 600$ mT, I_{sw} dependence on B_y and V_{G1} is measured and shown in Fig. 2(c). Four line cuts taken analogously as in Fig. 2(b) demonstrate that the supercurrent suppression inside the π region and the asymmetry between the 0 regions remain at high B_z, but is less prominent than at zero field. The high magnetic field causes a broadening of the π region along the V_{G1} axis [41]. We estimate that this expansion corresponds to $\sim$0.9 meV $\sim 4\Delta$ range in the junction electrochemical potential [53], noting that a same Zeeman energy $g\mu_B B \sim$ 0.9 meV would yield a g factor $g \sim 26$.

We proceed by studying the I_{sw} dependence on B_y and V_{G1} at higher gate voltages and $B_z = 0$ mT [Fig. 3(a)]. Two horizontal line cuts and one vertical line cut show that the supercurrent is enhanced around $V_{G1} = 2.49$ V, with a constant superconducting phase and an asymmetric amplitude modulation below and above the enhancement. Next, we apply B_z and remeasure the I_{sw} dependences at $B_z =$ 490 mT [Fig. 3(b), left] and $B_z = 720$ mT [Fig. 3(b), right]. At $B_z = 720$ mT, a π region is observed in the studied V_{G1} interval and two horizontal line cuts with comparable amplitudes indicate a weak suppression of the supercurrent in the π region. In addition, one vertical line cut shows that the asymmetry between the 0 regions is also weak. At $B_z = 490$ mT, two horizontal line cuts show that the frequency of I_{sw} oscillations doubles in a narrow V_{G1} interval. Such a double frequency oscillation has been studied theoretically [12,34,36] and observed experimentally [41], and is due to an intermediate regime existing in between a stable 0 and π region, here at $B_z = 0$ mT and $B_z = 720$ mT, respectively.

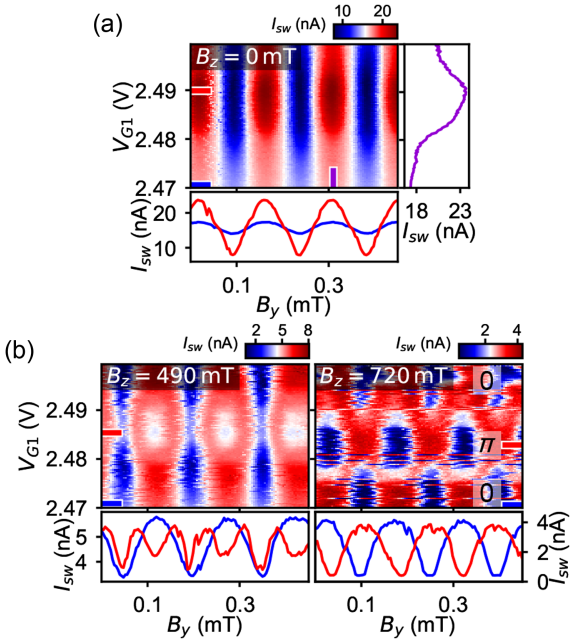

FIG. 3. I_{sw} as a function of B_y and V_{G1} at (a) $B_z = 0$ mT and (b) $B_z = 490$ mT (left) and $B_z = 720$ mT (right). The other gate voltages are $V_{L1} = V_{R1} = 1.75$ V, $V_{G2} = 2.88$ V, and $V_{L2} = V_{R2} = 1.75$ V. Horizontal line cuts (red and blue) are shown below and a vertical line cut (purple) is shown on the right.

Common features in Figs. 2 and 3 include the peculiarly sharp and asymmetric gate voltage dependence of the supercurrent amplitude in the narrow gate intervals associated with the $0-\pi$ transitions. Sharp dependences generally suggest that a localized state is involved, and in our experiment this is confirmed by the resonances in the normal-state conductance of the junction. The supercurrent and normal-state conductance generally remain finite when the localized state is off-resonant, which implies the existence of a background transport channel. This motivates us to explain the asymmetric resonant features by considering the interference between the localized state and direct transmission, as such mechanism gives rise to the peculiar asymmetry of Fano resonances [48]. In the rest of this Letter, we develop a model to theoretically investigate this effect.

Figure 4(a) (top) shows a schematic of a nanowire JJ with filled states in the leads and the transmission channel in black. Random potential minima in the junction are either filled (small solid regions) or empty (regions with dashed boundaries). An active localized state is shown in red. For convenience, we treat the direct-transmission channel as a resonance as well, but its energy broadening by far exceeds all other energy scales in the system. Therefore, we develop a two-dot model of a JJ, which is introduced in Fig. 4(a) (bottom). The first dot (red, energy E_1) represents the localized state. In order for the second dot (black, energy E_2) to model the transmission channel, the dot energies and tunnel couplings to the leads should satisfy the relation $\Gamma_2^{L,R}, E_2 \gg \Gamma_1^{L,R}, E_1$. Then, we can neglect the influence of the gate voltage and magnetic field on the second dot, and we also neglect its charging energy. Importantly, there is a direct tunnel coupling with the rate κ between the two dots that allows for the interference. Additional nontrivial elements are tunneling rates $\gamma_{L,R}$ that cannot be ascribed to a certain dot, but to a superposition state of the two dots. These parameters are at an intermediate scale, $\kappa, \gamma_{L,R} \simeq \sqrt{\Gamma_1 \Gamma_2}$. A magnetic field is introduced by the Zeeman energy in a simple form $\mathbf{B} \cdot \sigma$, where B is in the units of Δ. The spin-orbit length of the InSb nanowires is a few hundred nanometers [54], much longer than the length of the Josephson junction. Considering its weak influence, spin-orbit interaction is neglected in the main article. The charging energy U of the first dot is set to $U = 0$ for the simulation of Fig. 3. A more general case with $U > 0$ is presented and the influence of finite spin-orbit coupling is discussed in the extended

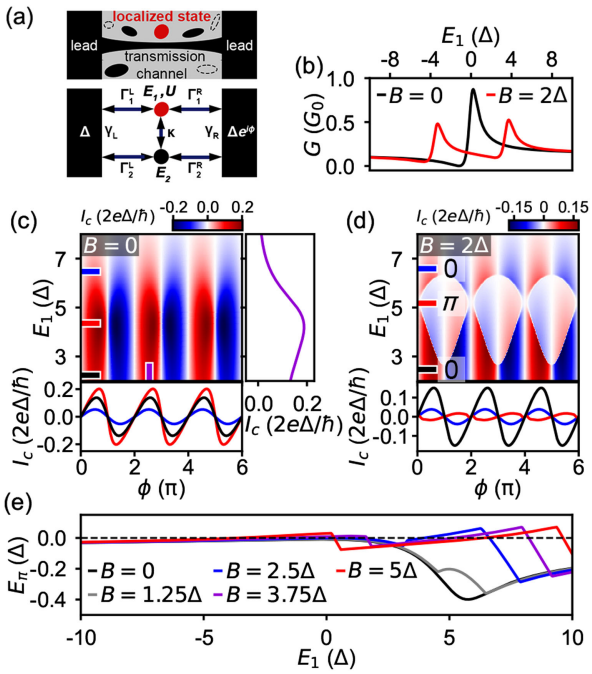

FIG. 4. (a) Schematic of the electron distribution in a nanowire JJ (top). Schematic of the two-dot model: the red dot (energy E_1, charging energy U) and the black dot (energy E_2, no charging energy) (bottom). Tunneling couplings to the leads (left, right) and between the dots are taken in ratios $\Gamma_1^L:\Gamma_1^R:\kappa = 0.001:0.001:1$ and $\Gamma_2^L:\Gamma_2^R:E_2 = 0.33:0.67:1.2$. (b) G as a function of E_1 for $B = 0$ (black) and $B = 2\Delta$ (red). (c) I_c (units $2e\Delta/\hbar$) as a function of ϕ and E_1 for $B = 0$. Horizontal line cuts (blue, red, and black) are shown below, and a vertical line cut (purple) is shown on the right. (d) Analogous to (c), but for $B = 2\Delta$. (e) E_π as a function of E_1 for different B. In (b)–(e), the charging energy is neglected by taking $U = 0$.

datasets in the Supplemental Material [53], where the full derivation of the model is given as well. The model parameters for the total resonant broadening, charging, and Zeeman energies can be extracted from the experiment [53] and have been taken consistently, while other parameters have been chosen to maximize the width of π regions though no extensive optimization has been made.

Figure 4(b) shows the normal-state conductance G through the two-dot system as a function of E_1 for $B = 0$ (black) and $B = 2\Delta$ (red). The ratio of the coupling rates is chosen such that the total coupling to the leads is $\Gamma = 4\Delta$ (as in the experiment) [53] and the two-dot interference results in the Fano shape of the resonant peculiarity due to competing processes of resonant transmission and resonant reflection [48]. The coupling parameters remain fixed in the rest of the Letter [53]. Next, we perform calculations on the supercurrent transport via the two coupled dots. The supercurrent is computed as a phase derivative of the total energy, including the contribution of the continuous spectrum. In Figs. 4(c) and 4(d), the junction CPR $I_c(\phi)$ is obtained as a function of E_1 for $B = 0$ and $B = 2\Delta$, respectively. For $B = 0$, three horizontal line cuts (blue, red, and black) and one vertical line cut (purple) show that the I_c amplitude is enhanced and asymmetrically modulated around the resonance. The CPR exhibits no phase shifts and is skewed at the resonance due to the enhanced transmission. For $B = 2\Delta$, a π region and two 0 regions are obtained along the E_1 axis, with supercurrent suppression in the π region and asymmetry between the 0 regions. In order to more easily identify π regions, we define a quantity $E_\pi = E(\phi = 0) - E(\phi = \pi)$ that is the difference between the junction ground state energies at $\phi = 0$ and $\phi = \pi$. Therefore, a π-shifted CPR is obtained whenever $E_\pi > 0$. Figure 4(e) displays E_π as a function of E_1 for different B. For small B, $E_\pi < 0$ for all E_1, confirming the absence of π shifts at $B = 0$. However, if B is sufficiently large, one obtains intervals in E_1 with $E_\pi > 0$. These intervals correspond to a π region that appears due to the Zeeman energy, as in Fig. 4(d). As B increases, the intervals of E_1 with $E_\pi > 0$ extend, which indicates that the π region broadens with the Zeeman energy.

The theoretical model reproduces the experimentally observed magnetic-field-driven $0-\pi$ transitions with supercurrent suppression inside the π regions and asymmetrical modulation outside the π regions. $0-\pi$ transitions at zero magnetic field are also reproduced by the model with a sufficiently large on-site interaction (the case of Fig. 2) and the typical features of suppressed supercurrent inside the π regions and the asymmetrical modulation outside the π regions still remain (see Fig. S8 [53]). In the calculations, I_c jumps show up due to the Andreev levels crossing the Fermi energy and changing the ground state parity of the junction. In the experiment, however, the sharp jumps are smeared out since the switching current I_{sw} close to parity transitions represents an average of the two parities.

In conclusion, we report on the CPR properties of an InSb-Al nanowire JJ in high magnetic fields. The supercurrent of the device is sharply and asymmetrically modulated in narrow intervals of the junction electrochemical potential, where a localized state is involved in the transport. In these intervals, high parallel magnetic fields can drive $0-\pi$ transitions with π shifted CPR in between two 0 regions. The $0-\pi$ transitions are favored by the on-site interaction in the localized state and can also occur at zero magnetic field. These phenomena can be explained by a theoretical model that involves a direct transmission channel and a localized state inside a JJ. The interference between the direct transmission channel and the localized state leads to Fano-resonance features as in the experiment. Our study thus introduces a superconducting counterpart of the Fano effect and shows how such effect can lead to $0-\pi$ transitions in high magnetic fields.

We thank Ghada Badawy, Sasa Gazibegovic and Erik P. A. M. Bakkers for growing the InSb nanowires.

We thank Raymond Schouten, Olaf Benningshof, and J. Mensingh for valuable technical support. This work has been financially supported by the Dutch Organization for Scientific Research (NWO), Microsoft Corporation Station Q and the European Research Council (ERC) under the European Union's Horizon 2020 research and innovation program (Grant Agreement No. 694272).

*Corresponding author: y.v.nazarov@tudelft.nl
†Corresponding author: wangjiyinshu@gmail.com

[1] B. D. Josephson, Phys. Lett. **1**, 251 (1962).
[2] E. Prada, P. San-Jose, M. W. A. de Moor, A. Geresdi, E. J. H. Lee, J. Klinovaja, D. Loss, J. Nygård, R. Aguado, and L. P. Kouwenhoven, Nat. Rev. Phys. **2**, 575 (2020).
[3] F. Pientka, A. Keselman, E. Berg, A. Yacoby, A. Stern, and B. I. Halperin, Phys. Rev. X **7**, 021032 (2017).
[4] M. Hell, M. Leijnse, and K. Flensberg, Phys. Rev. Lett. **118**, 107701 (2017).
[5] C. Schrade, S. Hoffman, and D. Loss, Phys. Rev. B **95**, 195421 (2017).
[6] J. Cayao, P. San-Jose, A. M. Black-Schaffer, R. Aguado, and E. Prada, Phys. Rev. B **96**, 205425 (2017).
[7] C. Schrade and L. Fu, Phys. Rev. Lett. **121**, 267002 (2018).
[8] A. Fornieri, A. M. Whiticar, F. Setiawan, E. Portolés, A. C. C. Drachmann, A. Keselman, S. Gronin, C. Thomas, T. Wang, R. Kallaher, G. C. Gardner, E. Berg, M. J. Manfra, A. Stern, C. M. Marcus, and F. Nichele, Nature (London) **569**, 89 (2019).
[9] H. Ren, F. Pientka, S. Hart, A. T. Pierce, M. Kosowsky, L. Lunczer, R. Schlereth, B. Scharf, E. M. Hankiewicz, L. W. Molenkamp, B. I. Halperin, and A. Yacoby, Nature (London) **569**, 93 (2019).
[10] M. C. Dartiailh, W. Mayer, J. Yuan, K. S. Wickramasinghe, A. Matos-Abiague, I. Žutić, and J. Shabani, Phys. Rev. Lett. **126**, 036802 (2021).
[11] T. Yokoyama, M. Eto, and Y. V. Nazarov, J. Phys. Soc. Jpn. **82**, 054703 (2013).
[12] T. Yokoyama, M. Eto, and Y. V. Nazarov, Phys. Rev. B **89**, 195407 (2014).
[13] D. B. Szombati, S. Nadj-Perge, D. Car, S. R. Plissard, E. P. A. M. Bakkers, and L. P. Kouwenhoven, Nat. Phys. **12**, 568 (2016).
[14] E. Strambini, A. Iorio, O. Durante, R. Citro, C. Sanz-Fernández, C. Guarcello, I. V. Tokatly, A. Braggio, M. Rocci, N. Ligato, V. Zannier, L. Sorba, F. S. Bergeret, and F. Giazotto, Nat. Nanotechnol. **15**, 656 (2020).
[15] J.-Y. Wang, C. Schrade, V. Levajac, D. van Driel, K. Li, S. Gazibegovic, G. Badawy, R. L. M. O. het Veld, J. S. Lee, M. Pendharkar, C. P. Dempsey, C. J. Palmstrøm, E. P. A. M. Bakkers, L. Fu, L. P. Kouwenhoven, and J. Shen, Sci. Adv. **8**, eabm9896 (2022).
[16] C.-Z. Chen, J. J. He, M. N. Ali, G.-H. Lee, K. C. Fong, and K. T. Law, Phys. Rev. B **98**, 075430 (2018).
[17] H. F. Legg, D. Loss, and J. Klinovaja, Phys. Rev. B **106**, 104501 (2022).
[18] R. S. Souto, M. Leijnse, and C. Schrade, Phys. Rev. Lett. **129**, 267702 (2022).
[19] H. Wu, Y. Wang, Y. Xu, P. K. Sivakumar, C. Pasco, U. Filippozzi, S. S. P. Parkin, Y.-J. Zeng, T. McQueen, and M. N. Ali, Nature (London) **604**, 653 (2022).
[20] C. Baumgartner, L. Fuchs, A. Costa, S. Reinhardt, S. Gronin, G. C. Gardner, T. Lindemann, M. J. Manfra, P. E. F. Junior, D. Kochan, J. Fabian, N. Paradiso, and C. Strunk, Nat. Nanotechnol. **17**, 39 (2022).
[21] B. Turini, S. Salimian, M. Carrega, A. Iorio, E. Strambini, F. Giazotto, V. Zannier, L. Sorba, and S. Heun, Nano Lett. **22**, 8502 (2022).
[22] G. Mazur, N. van Loo, D. van Driel, J.-Y. Wang, G. Badawy, S. Gazibegovic, E. P. A. M. Bakkers, and L. P. Kouwenhoven, arXiv:2211.14283.
[23] B. Zhang, Z. Li, V. Aguilar, P. Zhang, M. Pendharkar, C. Dempsey, J. S. Lee, S. D. Harrington, S. Tan, J. S. Meyer, M. Houzet, C. J. Palmstrom, and S. M. Frolov, arXiv:2212.00199.
[24] G. de Lange, B. van Heck, A. Bruno, D. J. van Woerkom, A. Geresdi, S. R. Plissard, E. P. A. M. Bakkers, A. R. Akhmerov, and L. DiCarlo, Phys. Rev. Lett. **115**, 127002 (2015).
[25] T. W. Larsen, K. D. Petersson, F. Kuemmeth, T. S. Jespersen, P. Krogstrup, J. Nygård, and C. M. Marcus, Phys. Rev. Lett. **115**, 127001 (2015).
[26] L. Casparis, M. R. Connolly, M. Kjaergaard, N. J. Pearson, A. Kringhoj, T. W. Larsen, F. Kuemmeth, T. Wang, C. Thomas, S. Gronin, G. C. Gardner, M. J. Manfra, C. M. Marcus, and K. D. Petersson, Nat. Nanotechnol. **13**, 915 (2018).
[27] A. Zazunov, V. S. Shumeiko, E. N. Bratus', J. Lantz, and G. Wendin, Phys. Rev. Lett. **90**, 087003 (2003).
[28] N. M. Chtchelkatchev and Y. V. Nazarov, Phys. Rev. Lett. **90**, 226806 (2003).
[29] C. Janvier, L. Tosi, L. Bretheau, C. O. Girit, M. Stern, P. Bertet, P. Joyez, D. Vion, D. Esteve, M. F. Goffman, H. Pothier, and C. Urbina, Science **349**, 1199 (2015).
[30] M. Hays, V. Fatemi, K. Serniak, D. Bouman, S. Diamond, G. de Lange, P. Krogstrup, J. Nygård, A. Geresdi, and M. H. Devoret, Nat. Phys. **16**, 1103 (2020).
[31] M. Hays, V. Fatemi, D. Bouman, J. Cerrillo, S. Diamond, K. Serniak, T. Connolly, P. Krogstrup, J. Nygaåd, A. L. Yeyati, A. Geresdi, and M. H. Devoret, Science **373**, 430 (2021).
[32] M. Pita-Vidal, A. Bargerbos, R. Žitko, L. J. Splitthoff, L. Grünhaupt, J. J. Wesdorp, Y. Liu, L. P. Kouwenhoven, R. Aguado, B. van Heck, A. Kou, and C. K. Andersen, Nat. Phys. **19**, 1110 (2023).
[33] B. I. Spivak and S. A. Kivelson, Phys. Rev. B **43**, 3740(R) (1991).
[34] E. Vecino, A. Martín-Rodero, and A. L. Yeyati, Phys. Rev. B **68**, 035105 (2003).
[35] T. Meng, S. Florens, and P. Simon, Phys. Rev. B **79**, 224521 (2009).
[36] M. Lee, R. López, H. Q. Xu, and G. Platero, Phys. Rev. Lett. **129**, 207701 (2022).
[37] J. A. van Dam, Y. V. Nazarov, E. P. A. M. Bakkers, S. D. Franceschi, and L. P. Kouwenhoven, Nature (London) **442**, 667 (2006).
[38] H. I. Jørgensen, T. Novotný, K. Grove-Rasmussen, K. Flensberg, and P. E. Lindelof, Nano Lett. **7**, 2441 (2007).

[39] E. J. H. Lee, X. Jiang, M. Houzet, R. Aguado, C. M. Lieber, and S. D. Franceschi, Nat. Nanotechnol. **9**, 79 (2014).
[40] S. Li, N. Kang, P. Caroff, and H. Q. Xu, Phys. Rev. B **95**, 014515 (2017).
[41] A. Bargerbos, M. Pita-Vidal, R. Žitko, J. Ávila, L. J. Splitthoff, L. Grünhaupt, J. J. Wesdorp, C. K. Andersen, Y. Liu, L. P. Kouwenhoven, R. Aguado, A. Kou, and B. van Heck, PRX Quantum **3**, 030311 (2022).
[42] A. Eichler, R. Deblock, M. Weiss, C. Karrasch, V. Meden, C. Schönenberger, and H. Bouchiat, Phys. Rev. B **79**, 161407(R) (2009).
[43] R. Maurand, T. Meng, E. Bonet, S. Florens, L. Marty, and W. Wernsdorfer, Phys. Rev. X **2**, 011009 (2012).
[44] B.-K. Kim, Y.-H. Ahn, J.-J. Kim, M.-S. Choi, M.-H. Bae, K. Kang, J. S. Lim, R. López, and N. Kim, Phys. Rev. Lett. **110**, 076803 (2013).
[45] A. M. Whiticar, A. Fornieri, A. Banerjee, A. C. C. Drachmann, S. Gronin, G. C. Gardner, T. Lindemann, M. J. Manfra, and C. M. Marcus, Phys. Rev. B **103**, 245308 (2021).
[46] P. San-Jose, E. Prada, and R. Aguado, Phys. Rev. Lett. **112**, 137001 (2014).
[47] C.-X. Liu, B. van Heck, and M. Wimmer, Phys. Rev. B **103**, 014510 (2021).
[48] U. Fano, Phys. Rev. **124**, 1866 (1961).
[49] S. Heedt, M. Quintero-Pérez, F. Borsoi, A. Fursina, N. van Loo, G. P. Mazur, M. P. Nowak, M. Ammerlaan, K. Li, S. Korneychuk, J. Shen, M. Y. van de Poll, G. Badawy, S. Gazibegovic, N. de Jong, P. Aseev, K. van Hoogdalem, and E. P. A. M. B. L. P. Kouwenhoven, Nat. Commun. **12**, 4914 (2021).
[50] F. Borsoi, G. P. Mazur, N. van Loo, M. P. Nowak, L. Bourdet, K. Li, S. Korneychuk, A. Fursina, J.-Y. Wang, V. Levajac, E. Memisevic, G. Badawy, S. Gazibegovic, K. van Hoogdalem, E. P. A. M. Bakkers, L. P. Kouwenhoven, S. Heedt, and M. Quintero-Pérez, Adv. Funct. Mater. **31**, 2102388 (2021).
[51] V. Levajac, G. P. Mazur, N. van Loo, F. Borsoi, G. Badawy, S. Gazibegovic, E. P. A. M. Bakkers, S. Heedt, L. P. Kouwenhoven, and J.-Y. Wang, Nano Lett. **23**, 4716 (2023).
[52] D. J. van Woerkom, A. Geresdi, and L. P. Kouwenhoven, Nat. Phys. **11**, 547 (2015).
[53] See Supplemental Material at http://link.aps.org/supplemental/10.1103/PhysRevLett.132.176304 for measurement setup, experimental parameter extraction, theoretical model, elaboration figures, additional calculations with finite charging energy, and explanation on data selection.
[54] I. van Weperen, B. Tarasinski, D. Eeltink, V. S. Pribiag, S. R. Plissard, E. P. A. M. Bakkers, L. P. Kouwenhoven, and M. Wimmer, Phys. Rev. B **91**, 201413(R) (2015).